SYNTHESIS AND CHARACTERISATION OF ESCULETIN LOADED CHITOSAN NANOPARTICLES (ESC-CNPs) AGAINST BREAST CANCER CELL LINE (MDA-MB-231) *INVITRO* STUDY

T. Siva Sankari[1], R.Subashini*

[1](Deparment of Biochemistry and Biotechnology,Annamalai University ,Chidambaram, Tamilnadu,India,stssankari@gmail.com)

Corresponding author

Dr.R. Subashini M.Sc.,M.Phil.,Ph.D,FSAB,

Assistant Professor, Deparment of Biochemistry,

D.G.Govt.Arts College for Women (Annamalai University),

Mayiladuthurai,609001

Tamilnadu,India

drrsubashini2023@gmail.com

Abstract

Breast cancer is the most prevalent cancer diagnosed globally, and its burden has increased over the past several decades. The mortality and morbidity rates of breast cancer cannot be reduced, despite advancements in early detection and improved treatment methods. The goal of the current study was to synthesize esculetin-loaded chitosan nanoparticles (ESC-CNPs) and analyze them using several distinguishing techniques, including UV-vis spectroscopy, SEM, FT-IR, and XRD, Cell viability, apoptotic morphological changes caused by AO/EtBr, changes in mitochondrial membrane potential (MMP), lipid peroxidation status (TBARS), antioxidants (SOD, GSH, and CAT), and ROS production were also used to investigate the anticancer effect of ESC-CNPs against MDA-MB-231 cells. Furthermore, qRT-PCR methods were used to assess the expression of apoptotic genes including Bax and Bcl-2. We discovered that the synthesized ESC-CNPs have an irregular spherical shape, are crystalline, and contain several functional groups. In addition, we discovered that ESC-CNPs treatments caused cell death in breast cancer cells. Apoptotic morphological abnormalities were assessed by AO/EtBr, and lipid peroxidation, antioxidants, and cell cycle arrest were found. Apoptosis markers were identified to confirm the molecular mechanism by which ESC-CNPs trigger apoptosis by altering gene expression.

Keywords: Antioxidant, Breast cancer, Chitosan nanoparticles, Esculetin, MDA-MB-231cells

Introduction

Cancer is a complicated illness with many pathological hallmarks, such as aberrant cell growth, invasion, and metastasis. Unrestrained cellular proliferation increases the number of aberrant cells; these cells enter the bloodstream, invade healthy organs, and cause secondary cancers to form. Breast cancer is the most frequent malignancy in women and the second greatest cause of cancer-related death [1, 2]. It has been found in half of the world's developed countries. [3]. Following the discovery of primary breast cancer, lymph nodes, the lungs, the liver, the bones, and the brain are the most common sites where metastases arise. However, metastases can develop at any site [4-5]. It is estimated that breast cancer will result in 6,85,000 deaths and 2.3 million new cases (11.7%) in 2020[6]. The majority of cancers are currently treated with a mix of surgical resection, radiation therapy, chemotherapy, and immunotherapy. [7]. These medicines do, however, have some side effects, including general toxicity, vomiting, and hair loss. Therefore, it is incumbent upon scientists to utilise the expanding understanding regarding the development of the subsequent generation of targeted medicines. Recent years have seen nanotherapeutics play a significant role in the side-effect-free treatment of many cancers.

Nanoparticles (100 nm particles) can be employed efficiently within the tumour microenvironment, where they passively accumulate and improve permeability and retention [8,9]. Nanoparticles can be manufactured utilizing several ways due to their unique properties [10, 11]. The size, shape, and surface morphology of nanoparticles have a significant impact on their physical, chemical, optical, and electrical properties [12]. Nanoparticles can be metallic or nonmetallic (polymeric). Polymeric nanoparticles, on the other hand, can transport medicines, proteins, and DNA to specific cells and organs. Their size promotes Metal and non-metal nanoparticles (polymeric) are both possible types. Stability in the bloodstream and efficient penetration via cell membranes. Scientists have become interested in chitosan because of its distinct features among other polymers [13].

Chitosan [(1, 4)-2-amino-2-deoxy-D-glucan] is the second most common natural biopolymer and is formed by N-deacetylating chitin. Furthermore, it is easily processed into a wide range of forms, such as films, threads, tablets, membranes, and microscopic particles and nanoparticles, and it is abundant [14]. Chitosan nanoparticles are extremely effective at drug capture [15].Esculetin (6, 7-dihydroxy coumarin), a catecholic coumarin found naturally in a variety of medicinal plants including Artemisia capillaries, Citrus limonia, and Euphorbia lathyris, is extensively dispersed

(16). Esculetin and its derivatives have been proven in vitro to be effective against a wide range of tumors and to inhibit the proliferation of many human malignant cell lines. (17-20). additionally, it increases the apoptosis that taxol causes in human hepatocellular carcinoma cells (HepG2) (21). Additionally, esculetin has several biological effects, including DNA protection, inhibition of lipoxygenase, free radical scavenging and cancer Chemoprevention [22-25].

In this study, esculetin-loaded chitosan nanoparticles were produced (ESC-CNPs). The esculetin-loaded chitosan nanoparticles were further examined by ultraviolet (UV), Fourier transform infrared (FTIR), scanning electron microscopy (SEM) and X-ray powder diffraction (XRD). In addition, the cytotoxic effect of ESC-CNPs against human breast cancer cell lines was evaluated (MDA-MB-231).

1. Materials and methods

2.1. Chemicals

From Sigma-Aldrich Chemicals Private Ltd. (Bangalore, India), chitosan, acetic acid, and esculetin were all purchased. DMSO, Tissue culture medium, MTT, antibiotic, trypsin, FBS, MTT, ethidium bromide, acridine orange, Rhodamine-123, DAPI, carboxy-H2DCFDA were acquired from HiMedia Laboratories, Mumbai. The existing chemicals and solvents used were of molecular and analytical grade.

2.2. Synthesis of ESC-CNPs

Ionic gelation was used to create ESC-CNPs, as suggested by Calvo et al. [23]. 100 mg of chitosan were dissolved in 100 ml of 2% acetic acid, and they were agitated on a magnetic stirrer overnight to prepare a chitosan stock solution. In 30 ml of deionized water dissolve in 15 mg of sodium tripolyphosphate (TPP) to create a solution. Similarly, 10 mg of esculetin was dissolved in 10 mL of DMSO to form an esculetin stock solution. To prepare ESC-CNPs, 30 ml of chitosan solution and 10 ml of esculetin solution were combined in a beaker and spun for a short period to equally distribute the esculetin. The mixture was then constantly agitated on a magnetic stirrer for 60 minutes, or until the formation of chitosan nanoparticle suspension was indicated by a change in color. For 15 minutes, the entire suspension was centrifuged at 16,000 rpm in a tube. After centrifugation, the supernatant was removed, and the ESC-CNPs pellet was stored in a freezer at 4 °C for later use. The entire surgery was done in complete darkness.

2.3. Characterization of ESC-CNPs

The crystal size of ESC-CNPs was determined using XRD (X-ray diffraction). The absorbances and surface functional groups associated with the synthesised CNPs and ESC-CNPs were examined using the UV-Vis (ultraviolet-visible) spectrophotometer and the FTIR (Fourier transform infrared spectrophotometer, respectively). SEM was used to study the structure of ESC-CNPs.

2.4 pH-sensitive *in vitro* drug release study

The drug release profile of produced esculetin loaded chitosan nanoparticles at two pH levels, 7.0 and 5.0, was examined. The esculetin-loaded chitosan nanoparticles were mixed in PBS (pH 7.0) before being placed in a dialysis bag. The dialysis bag was submerged in 95 ml of PBS with pH levels of 5.0 and 7.0 while being shaken. Performing the drug release profile at 37° C. The aqueous solution was removed and 5 ml of fresh PBS was added at regular intervals. The amount of drug released was calculated by measuring the absorbance of esculetin at 295 nm with a UV-visible spectrophotometer.

2.5. Cell culture

The MDA-MB-231 human breast cancer cell line was purchased from NCCS Pune in India. The Dulbecco's Modified Eagle's Medium (DMEM) with 10% FBS and antibiotics was used to grow and maintain the MDA-MB-231 cell line in culture flasks at 37°C in a humidified atmosphere with 5% CO2.

2.6. MTT assay

The cell viability of MDA-MB-231 was evaluated using 3-(4,5-dimethylthiazol-147 2-yl)-2,5-diphenyl-tetrazolium bromide (MTT). Cells were seeded at a concentration of $1x10^4$ cells/well in microtiter plates. Seeded wells were treated for 24 hours in triplicate with ESC-CNPs at doses of 5, 10, 20, 40, and 80 µg/ml, while the remaining wells were left untreated to serve as controls. Following incubation, the culture medium was replaced with 150 µl of fresh media and 50 µl of MTT (5 mg/mL in PBS), and the plate was incubated for 4 hours at 37 °C in a humidified atmosphere with 5% CO_2. The formed formazan crystals were dissolved in 200 µl of DMSO. The plate was incubated for 30 mins at 37 °C before the optical density was measured at 540 nm with a spectrophotometric microplate reader. The IC50 and IC90 values were calculated from the sample dose-response curve, which showed inhibition of 50% and 90% cytotoxicity relative to

control cells, respectively. All experiments were carried out in triplicate to ensure the accuracy and reliability of the data.

2.7. Biochemical analysis

MDA-MB-231 cells were incubated for 24 hours with or without ESC-CNPs. The cells were then rinsed with PBS, scraped, lysed, and centrifuged at 12000 rpm for 15 minutes at 4 °C to collect the supernatant, which may then be used to evaluate oxidative stress markers. According to Ohkawa et al. 1979[26], the amount of TBARS was measured to determine the amount of lipid peroxide. Kakkar et al. [27] evaluated the activity of superoxide dismutase (SOD) in 1984. Sinha (1972) [28] calculated the activity of catalase (CAT). According to Ellman's (1959) [29] techniques, the activity of reduced glutathione (GSH) was evaluated. Biochemical alterations were compared with untreated cells.

2.8. Intracellular ROS determination

The stress responses of MDA-MB-231 cells subjected to ESC-CNPs were detected using the oxidative-sensitive dye 2′7′-dichlorodihydro-florescenceindiacetate (DCFH-DA). Cells were diluted into a 6-well plate with a cover slip, treated with ESC-CNPs, and incubated at 37 °C for 24 hours. The coverslip was removed from the 6-well plate after incubation, and the cells were stained for 30 minutes with 100 l of DCFH-DA to evaluate ROS production. The control cells were co-cultured MDA-MB-231 cells that had not been stained with DCFH-DA. After incubation, the dyed coverslip was rinsed with PBS, and the differentiation of treated and untreated cells was studied under a fluorescence microscope.

2.9. Determination of mitochondrial membrane potential

Rhodamine-123 dye was used to evaluate mitochondrial membrane potential in MDA-MB-231 cells. MDA-MB-231 cells (1104 cells) were treated for 24 hours with ESC-CNPs. The dye rhodamine-123 (1 mg/ml) was added 2 hours before the experiment finished. After being rinsed with PBS, the cells were studied under a fluorescence microscope.

2.10. Acridine orange/ethidium bromide dual staining

ESC-CNPs were used to label MDA-MB-231 cells with the fluorescent dyes acridine orange and ethidium bromide (AO/EB). Each well of a 6-well plate was seeded with 1x104 cells, which were then incubated overnight. Following an untreated period of roughly 24 hours, the cells were given ESC-CNPs. After treatment, cells were rinsed with ice-cold PBS, and each well was incubated for 8-10 minutes at 37°C with a dual AO/EB fluorescent staining solution. The extra colour was

subsequently removed from PBS. Images of tagged cells were counted and evaluated under a fluorescent microscope in 15 to 20 minutes.

2.11. DAPI staining

MDA-MB-231 cells were grown in six-well plates and treated for 24 hours with ESC-CNPs. Trypsinization was used to harvest the cells, which were subsequently fixed in 100% ethanol overnight at -20 C. The cells were rinsed three times with ice-cold PBS before being fixed for 10 minutes at room temperature in a 1 ml methanol solution. At room temperature and in the dark, the fixed cells were dyed with a 1 mg/ml DAPI solution and placed on glass slides. The morphology of cells was studied using a fluorescent microscope.

2.12. qRT-PCR

The levels of Bax (TTTGCTTCAGGGTTTCATCC and GCCACTCGGAA AAAGACCT C) and Bcl-2 (GATGTCGCCCCTGGTGGACAAC and CACCAGGGCCAAACTGAGCAGAG) in both untreated and ESC-CNPs-treated cells were determined using quantitative real-time PCR (qRT-PCR). The RNeasy kit (Qiagen, USA) was used to extract RNA, and 1 l of the extracted RNA was reverse-transcribed into cDNA. The PCR amplification technique used in a thermocycler was denaturation at 95°C for 25 seconds, annealing at 55°C for 25 seconds, and extension at 72°C for 30 seconds. To normalize the expression levels, actin (GATGATGATATCGCCGCGCT and CCTCGTCGCCCACATAGGAA) was used as a reference gene. The fold change was calculated using the comparative threshold cycle (Ct) method. The gene expression level for each gene was determined using the 2^-ΔΔCt technique in triplicate experiments.

2.13. Statistical analysis

The results of the trials in the study were evaluated using one-way ANOVA and Duncan's multiple range test (DMRT) in SPSS version 21.0 for Windows. All values were reported as means standard deviations. If the p 0.05, the results were judged statistically significant.

3.RESULTS

3.1. Characterisation of Esculetin loaded Chitosan Nanoparticles

3.1.1. UV-Visible spectra

Fig. 1 depicts the UV spectrum of the UV-Visible spectra. A band of absorption was seen between 300 and 400 nm. It was discovered that the wavelengths of pure CNPs and ESC-CNPs in its nanoparticles were 311 nm, 374 nm, and 361 nm, respectively. The synthesis of ESC-CNPs

revealed a maximum absorption peak at 300-400 nm in the UV spectrum, and Deepika et al., (2022) found a similar result [30].

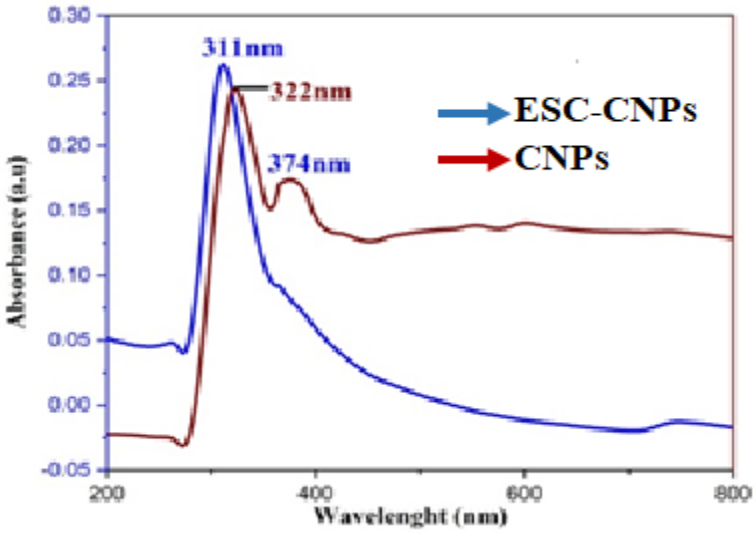

Fig.1. UV-Visible spectra for ESC-CNPs

3.1.2. XRD

Fig. 2 depicts the ESC-CNPs X-ray diffraction measurements show very broad peaks at 2 = 14.1°, 16.9°, 18.5°, 20.7°, 22.8°, and 26.8° (Figure 2). However, the chitosan peak at 2 = 20° vanished, and the very broad peak at 2 = 20° became modest in ESC-CNPs. These findings indicate that ESC-CNPs are compatible, resulting in the production of ESC-CNPs. The XRD pattern also revealed that the ESC-CNPs derivative is amorphous, which could be useful in biological applications. These findings are consistent with previous studies that demonstrated the creation of nanoparticles utilising chitosan [31]. According to Wan et al (2003).

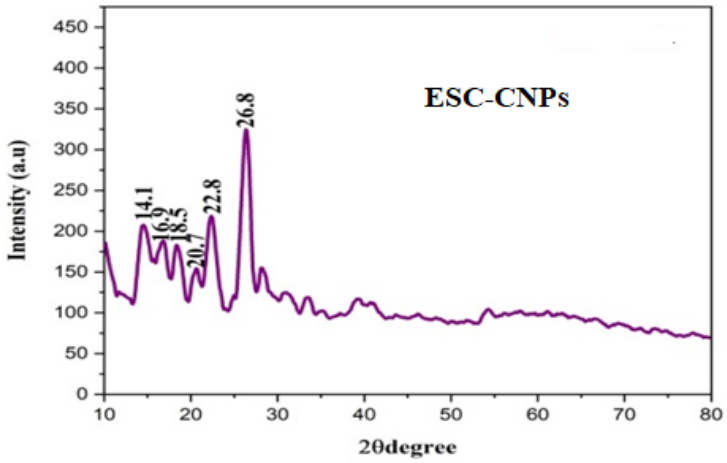

Fig.2. XRD for ESC-CNPs

3.1.3. FTIR spectra

Fig. 3 depicts the FTIR spectra of ESC-CNPs. Figure 1 shows a spectrum with multiple distinct peaks at 34581cm, 20831cm, 16391cm, and 7061cm. The characteristic peak of the ESC-CNPs derivative (Fig. 3) at 1639 cm1 is attributable to the formation of (C=N). The hydroxyl groups' O-H adsorption peak is 3458 cm1; 2083 cm1 (C-H stretch). The intensity of main alcohol 704 cm1 owing to C=O stretching vibration decreases significantly when compared to ESC-CNPs [32].

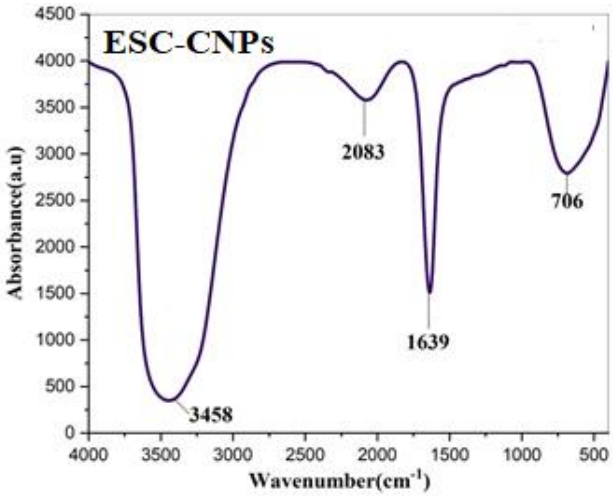

Fig.3. FTIR spectra of ESC-CNPs

3.1.4. SEM

The morphological structure of ESC-CNPs is shown in Fig. 4**.** The surface SEM images of chitosan and ESC-CNPs show distinct variations. Pure chitosan is mostly made up of platelet-like chitosan micro-fibrils of varying sizes. Although the surface structure of chitosan bases is compact and uniform, the surface roughness of ESC-CNPs was greater than that of esculetin irregular spherical structure. Interruption of the backbone of ESC-CNPs bases polymer can explain this observation as a result of the reactivity of ESC-CNPs amine groups with aromatic aldehydes and, most likely, due to the breaking of hydrogen bonds in the ESC-CNPs. As a result, the reaction of chitosan with aromatic resulted in extremely significant alterations in the surface morphology and crystallinity of the esculetin. SEM analysis of ESC-CNPs revealed that they were irregular spherical, which was consistent with previous reports [33].

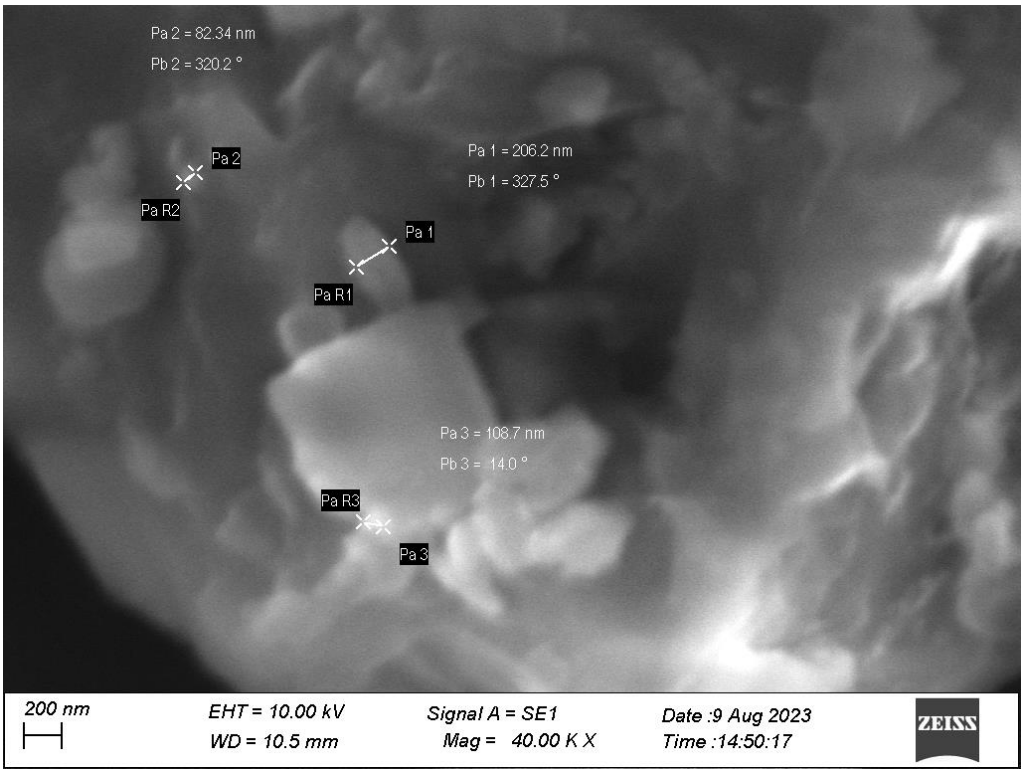

Fig.4. SEM of ESC-CNPs

3.1.5. *in vitro* drug release study

Fig. 5 depicts the in vitro esculetin release profile from the loaded chitosan nanoparticles. The findings show that esculetin-loaded chitosan nanoparticles have a misleading pH-responsive release pattern. In PBS, the esculetin-loaded chitosan nanoparticles released more than 88% of the integrated esculetin in about 17 hours (pH 5.0). The drug release ratio was comparable lower at the other pH 7.0 values than it was at pH 5.0. However, at pH 5.0, there was a fast release, which might have been caused by the bond between the drug esculetin and the chitosan nanoparticles deforming under the influence of the acidic pH. Tumours have a slightly higher acidic extracellular pH than blood and healthy tissue. Therefore, the specific pH 5.0 favours the drug's effective release more than pH 7.0.

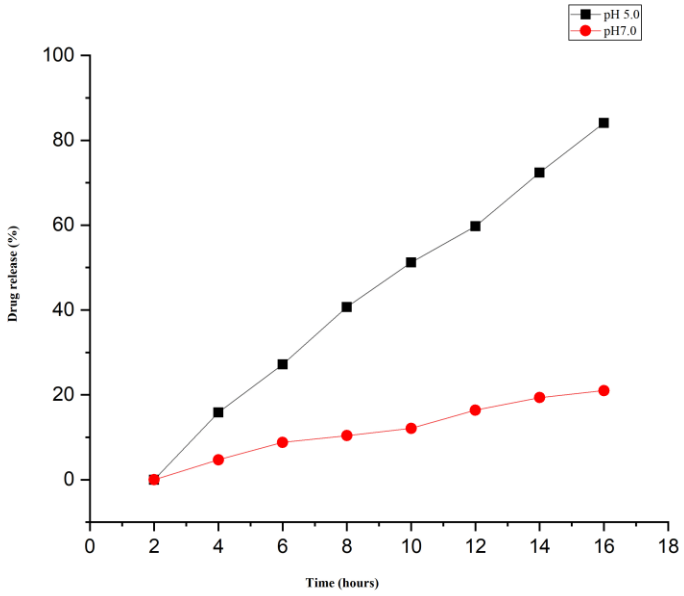

Fig.5. In vitro drug release profile of ESC-CNPs at pH 5.0 and 7.0

3.2. Anticancer potential of ESC-CNPs in MDA-MB-231 cells

The effect of ESC-CNPs on breast cancer cells was investigated by culturing MDA-MB-231 cells for 24 hours at various concentrations (5, 10, 20, 40, and 80 g/ml) and assessing cell viability using the MTT assay (Fig. 6). At increasing doses, ESC-CNPs suppressed cancer cell proliferation in MDA-MB-231 cells. The inhibitory concentrations (IC50 and IC90) of ESC-CNPs were

determined to be 19.12 ±0.55 g/ml and 76.81 ± 2.06 g/ml, respectively. The study's findings revealed that when the concentration of ESC-CNPs grew, cancer cell survival was reduced. According to the study's findings (control), ESC-CNPs were much more effective than untreated MDA-MB-231 cells in preventing cancer cell development and survival.

Fig. 7 showed the progressive morphological alterations of ESC-CNPs treated MDA-MB-231 cells, including cell shrinkage, membrane blebbing, chromatin cleavage, and nuclear condensation. Untreated cells with normal nuclei (smooth nuclei), organelles, and cell membranes.
Apoptosis plays an important function in determining cellular cytotoxicity after pharmacological therapy. [34, 35]. In this work, we discovered that breast cancer cells exhibited cell death in the MTT assay (Fig. 7). This indicated that ESC-CNPs could inhibit the proliferation of breast cancer cells.

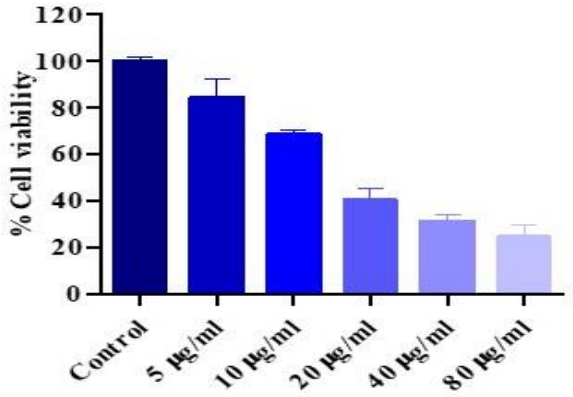

Fig 6. Effect of ESC-CNPs on the cytotoxicity of MDA-MB-231 cells by MTT assay

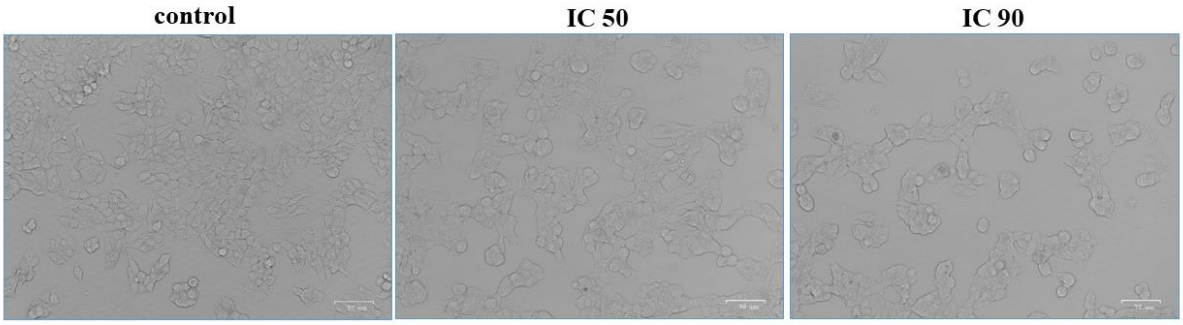

Fig. 7. Effect of ESC-CNPs on the morphological changes of MDA-MB-231 cells. Cells were treated with IC 50 and IC 90 concentrations of ESC-CNPs for 24 hours. The cell morphological changes were examined and photographed under phase contrast microscopy.

3.3. Effect of ESC-CNPs on antioxidant and lipid-peroxidation activity in MDA-MB-231 cells

To determine the antioxidant capacity of ESC-CNPs, we assessed lipid peroxidation (TBARS) and antioxidant enzyme status (SOD, CAT, and GSH) in MDA-MB-231 cells in Fig. 8. The SOD activity of cells treated with IC 50 and IC 90 doses of ESC-CNPs was measured to be7.69±0.78 and 4.36±0.31 U/mg protein, respectively. Comparatively, the SOD activity of untreated control cells was 15.19±0.49 U/mg protein. The CAT activity of untreated control cells was 14.16±0.71 U/mg protein, 8.90±0.13 U/mg protein, and 4.37±0.46 U/mg protein, respectively. The GSH activity of cells treated with IC 50 and IC 90 doses of ESC-CNPs were 12.57±0.61 and 7.58±0.39 U/mg, respectively. Comparatively, the GSH activity of untreated control cells was 3.36±0.47 U/mg protein.

In addition, the levels of TBARS, a measure of lipid peroxidation, increased considerably in MDA-MB-231 cells following treatment with ESC-CNPs. The IC 50 and IC 90 doses of ESC-CNPs were associated with TBARS values of 12.84±0.42 and 20.61±0.83m moles/mg protein, respectively. TBARS levels in untreated MDA-MB-231 control cells were 4.15±0.56.

Regular ingestion of antioxidant mediators appears to prevent or mitigate the negative consequences of long-term or acute, severe oxidative stress. Numerous studies have shown that different chemicals, such as free radical scavengers, can reduce or prevent oxidative cell damage [36]. Lipid peroxidation is a critical mechanism for oxidative stress. It has long been recognized that oxidative stresses induce significant cellular damage due to necrotic cell death caused by lipid peroxidation and alterations in proteins and nucleic acids. [37]. In this study, we found that ESC-

CNPs treated groups had elevated levels of TBARS compared to the untreated control groups. (Fig. 8). The increased TBARS were associated with decreased cell viability, which suggested that cell death was the primary factor causing the lipid peroxidation-induced membrane damage. According to several studies, antioxidant enzymes are crucial for protecting against mediators that cause tumours. Absorbing, cell malignancy or transformation was frequently associated with decreased activity of antioxidant enzymes such as catalase (CAT), superoxide dismutase (SOD), and reduced glutathione (GSH), which increased cellular sensitivity to pro-oxidant chemicals. [38]. We discovered that when we added ESC-CNPs to MDA-MB-231 cells, the status of antioxidant enzymes like SOD, GSH, and CAT reduced due to oxidative stress. (Fig. 8).

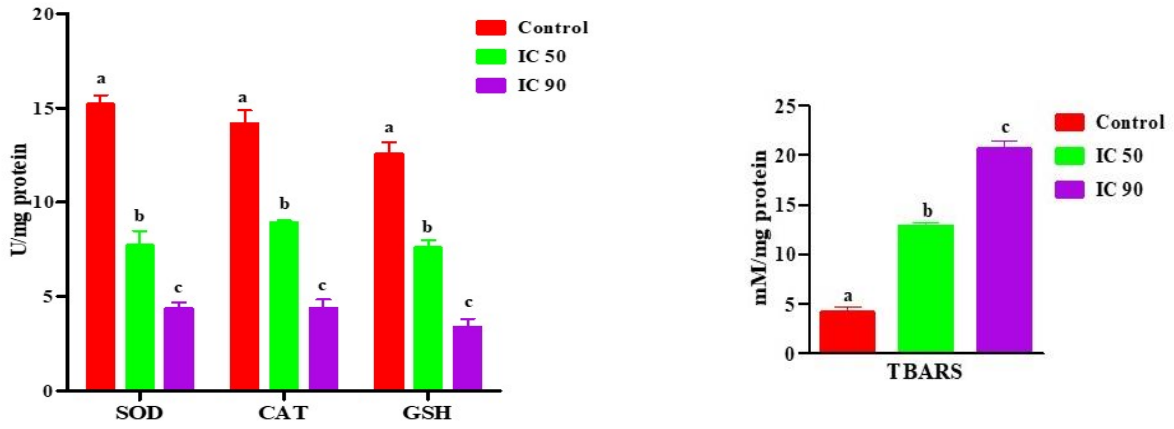

Fig. 8. **Effect of ESC-CNPs on the antioxidant (SOD, CAT, GPx) and lipid-peroxidation (TBARS) markers in MDA-MB-231 cells. Untreated control cells show increased antioxidant and decreased lipid-peroxidation levels. ESC-CNPs treated cell shows decreased antioxidant and increased lipid-peroxidation levels (IC 50 and IC 90). Values are given as means ± S.D. of three experiments in each group. Values not sharing a common marking (a, b, c) differ significantly at p<0.05 vs. control (DMRT).**

3.4. Effect of ESC-CNPs on ROS generation in MDA-MB-231cells

Microscopy revealed the generation of ROS in MDA-MB-231 cells (Fig. 9). According to the findings, ESC-CNPs are effective at reducing cancer cell viability. MDA-MB-231cells treated with ESC-CNPs were examined with the DCFH-DA dye, which emits green fluorescence. The study findings revealed that the cell's fluorescence strength and ROS production both increased, indicating that ESC-CNPs caused MDA-MB-231cells to undergo apoptosis, which was facilitated by ROS synthesis rather than untreated control cells.

ROS generation is required for pathogenic activities such as cell proliferation, oxidative defence systems, and pathogen death [39]. Cancer cells produce more ROS and trigger more apoptosis than normal cell lines [40]. As a result, the researchers discovered that ESC-CNPs can increase ROS production, increasing the rate of apoptosis and hastening cancer cell death.

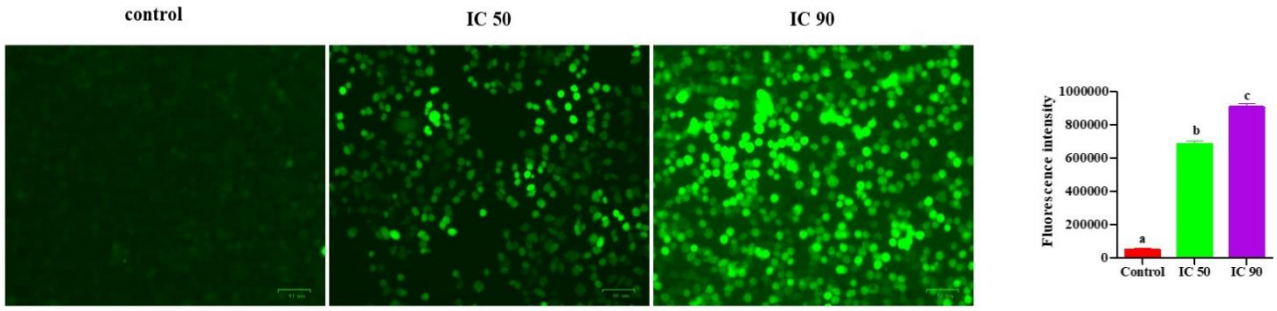

Fig. 9. **The Effect of ESC-CNPs on intracellular ROS generation was evaluated by using DCFH-DA staining in MDA-MB-231cells. The images were acquired using a fluorescent microscope. Values are given as means ± S.D. of three experiments in each group. Values not sharing a common marking (a, b, c) differ significantly at p<0.05 vs control (DMRT).**

3.5. Effect of ESC-CNPs on mitochondrial membrane potential (MMP)

Rh-123 dye was used to evaluate the changes in the membrane potential of the mitochondria in MDA-MB-231cells. Untreated control cells displayed enhanced green fluorescence, a sign of higher mitochondrial membrane potential. Additionally, cells treated with ESC-CNPs had greater mitochondrial membranes than untreated control cells (Fig. 10).

More research was conducted to investigate the induction of apoptosis in MDA-MB-231 cells by ESC-CNPs. Currently, cancer cell treatment is primarily focused on mitochondria to trigger

apoptosis. Among the numerous dyes available, Rh-123 is the most commonly used dye for detecting Mitochondrial Membrane Potential (MMP).

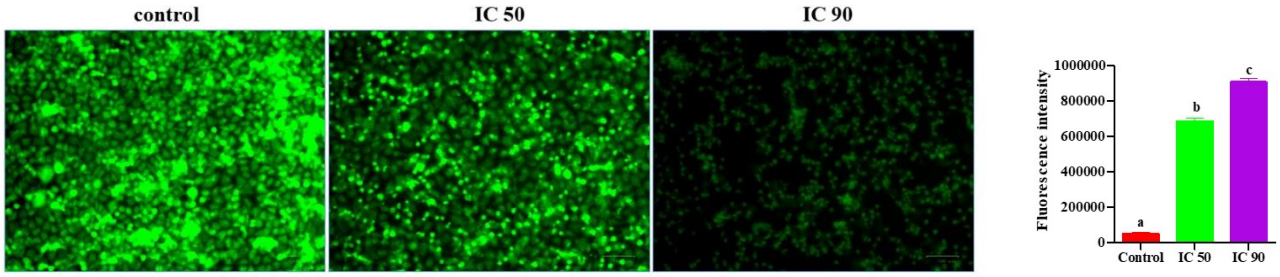

Fig. 10. **Fluorescent microscopic images of mitochondrial membrane potential using Rh-123 in MDA-MB-231cells treated with IC 50 and IC 90 doses of ESC-CNPs. The images were acquired using a fluorescent microscope. Values are given as means ± S.D. of three experiments in each group. Values not sharing a common marking (a,b,c) differ significantly at p<0.05 vs control (DMRT).**

3.6. Effect of ESC-CNPs on apoptosis induction in MDA-MB-231cells

The AO/EB stain can be used to identify apoptotic cells. Cells treated with ESC-CNPs at IC 50 and IC 90 dosages displayed typical apoptotic morphological changes such as nuclei fragmentation or nuclear shrinkage, condensed chromatin fragments, and shrinking cytoplasm. Figure 11 depicts the study's findings. Untreated control cells have normal nuclear architecture. Cells treated with ESC-CNPs appeared yellowish-orange in color. Treatment with ESC-CNPs dramatically boosted apoptosis and decreased the number of viable cells compared to untreated control cells.

The MDA-MB-231 cells treated with ESC-CNPs underwent apoptosis, which was validated by AO/EB staining in the current investigation.Cells have green nuclei, but cells that have undergone early apoptosis show bright green fluorescence. Condensed chromatin is depicted by green patches, whereas late apoptotic cells detected after ESC-CNPs therapy are represented by orange to red cells. Depolarized mitochondria are indicated by patches that seem opaque orange. All of the observed morphological changes indicate that the cells treated with ESC-CNPs have undergone apoptosis [41].

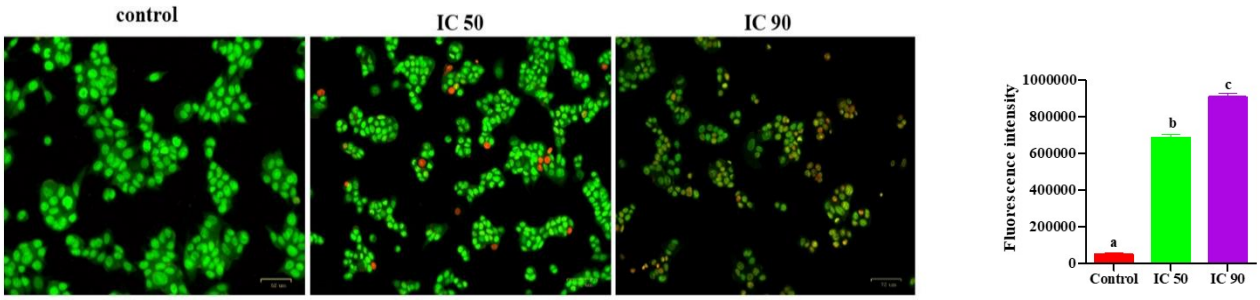

Fig. 11 **Detection of Apoptosis induced in MDA-MB-231cells treated with IC 50 and IC 90 doses of ESC-CNPs using AO/EB double staining. The images were acquired using a fluorescent microscope. Values are given as means ± S.D. of three experiments in each group. Values not sharing a common marking (a,b,c) differ significantly at p<0.05 vs control (DMRT).**

3.7. Effect of ESC-CNPs on nuclear alterations in MDA-MB-231 cells

To verify the nuclear fragmentation of ESC-CNPs on MDA-MB-231 cells, DAPI staining was performed. Fig. 12 depicts fluorescence microscopy images of MDA-MB-231 cancer cells stained for 24 hours with DAPI stain at the IC 50 and IC 90 concentrations of ESC-CNPs. The untreated cells exhibited no significant alterations, however, the ESC-CNPs-treated cells exhibited brighter intensity of fluorescence, indicating compacted chromatins and nuclear fragmentations than untreated cells.

DAPI staining confirms that ECS-CNPs treated MDA-MB-231 cells exhibit severe membrane breakdown and lack of cell adhesion. The nuclear-specific dye experiment demonstrates conclusively that ESC-CNPs generate evident alterations in the cellular and nuclear morphology, hence drastically reducing cell viability. This provides more evidence that particle-induced cell detachment is caused by the activation of membrane protein precipitation. As a result of their DNA breakage, necrotic cells exhibited a blue fluorescence. The toxicity induced by ESC-CNPs may be caused by oxidative stress, DNA damage, and induction of apoptosis.

Some other anticancer drugs like baicalein and Tamoxifen were loaded on chitosan nanoparticles induced apoptosis in MDA-MB-231 cells was also reported previously [42, 43].

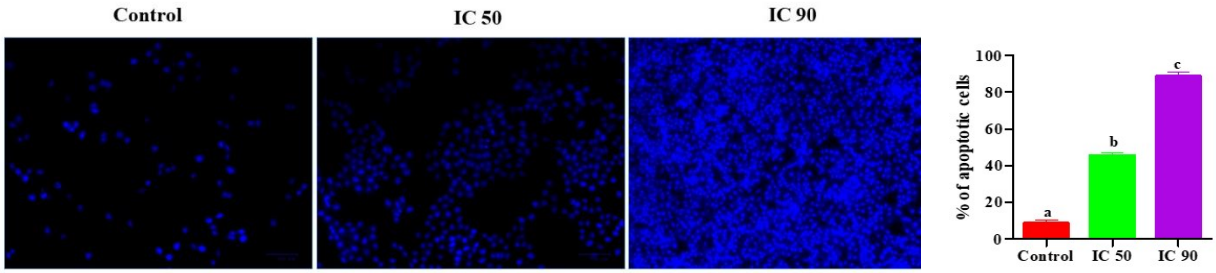

Fig. 12 **The effect of IC 50 and IC 90 doses of ESC-CNPs on nuclear alterations in MDA-MB-231 cells was investigated using DAPI staining. The images were acquired using a fluorescent microscope. Values are given as means ± S.D. of three experiments in each group. Values not sharing a common marking (a,b,c) differ significantly at p<0.05 vs control (DMRT).**

3.8. Effect of ESC-CNPs on Bax and Bcl-2 expression

Bcl-2 expression is increased in control cells, whereas Bax expression is lowered. In contrast, cells treated with ESC-CNPs showed pinned Bcl-2 and enhanced Bax expression. Control and ESC-CNPs-challenged MDA-MB-231 cells apoptotic gene expression statuses were displayed in Fig. 13.

Multiple variables, including tumour suppressor and inducer genes such as Bcl-2 family proteins, which may trigger tumour cell survival and provide resistance to apoptosis [44], tightly regulate the apoptotic pathway. This protein family contains the key regulators of endogenous mitochondrial apoptosis [45]. Bax's pro-apoptotic activity migrates from the cytoplasm to the mitochondrial outer membrane, altering its permeability and inducing the release of cytochrome c [46]. Furthermore, the Bcl-2 protein can control the opening and closing of MPTP. In our investigation, we found that ESC-CNPs therapy reduced the amount of Bcl-2 protein while raising the level of Bax (Fig. 13).

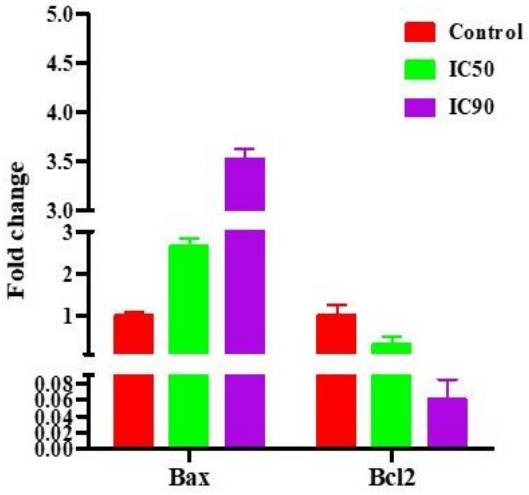

Fig. 13. **Effect of IC 50 and IC 90 doses of ESC-CNPs on apoptotic marker Bcl-2 and Bax expression analysed by qRT-PCR in MDA-MB-231cells. Values are given as means ± S.D. of three experiments in each group. Values not sharing a common marking (a, b, c) differ significantly at p<0.05 vs. control (DMRT).**

4. Conclusion

The current study aims to synthesise ESC-CNPs using the ionic gelation method. UV-visible spectroscopy validated the synthesis of esculetin-loaded chitosan nanoparticles, with the highest absorption of nanoparticles at 300 and 400 nm. SEM images revealed irregular spherical-shaped nanoparticles. The encapsulation of esculetin in chitosan nanoparticles was confirmed by FTIR. The MTT assay was used to investigate the anticancer activity of ESC-CNPs against MDA-MB-231 cell lines in vitro. Furthermore, ESC-CNPs inhibited MMP, elevated intracellular ROS levels, and boosted cytotoxicity in MDA-MB-231 cells. In addition, the ESC-CNPs induced apoptosis in MDA-MB-231 cell lines by boosting pro-apoptotic proteins and lowering anti-apoptotic proteins. ESC-CNPs were used as therapeutic approaches in this work to harness tumour microenvironment features by direct drug delivery to the targeted location.

5.Acknowledgement

This work received no fund from any funding agencies.

6.References

[1]. Grobmyer SR, Zhou G, Gutwein LG, Iwakuma N, Sharma P, Hochwald SN. Nanoparticle delivery for metastatic breast cancer. Nanomedicine: Nanotechnology, Biology and Medicine. 2012 Sep 1; 8:S21-30.

[2]. Menon JU, Ravikumar P, Pise A, Gyawali D, Hsia CC, Nguyen KT. Polymeric nanoparticles for pulmonary protein and DNA delivery. Acta biomaterialia. 2014 Jun 1; 10(6):2643-52.

[3]. Gold J, Winer EP. Chemotherapy for metastatic breast cancer. InThe Breast 2009 Jan 1 (pp. 1233-1261). WB Saunders.

[4]. Carty NJ, Foggitt A, Hamilton CR, Royle GT, Taylor I. Patterns of clinical metastasis in breast cancer: an analysis of 100 patients. European Journal of Surgical Oncology (EJSO). 1995 Dec 1; 21(6):607-8.

[5]. Suri SS, Fenniri H, Singh B. Nanotechnology-based drug delivery systems. Journal of occupational medicine and toxicology. 2007 Dec; 2:1-6.

[6]. Sung H, Ferlay J, Siegel RL, Laversanne M, Soerjomataram I, Jemal A, Bray F. Global cancer statistics 2020: GLOBOCAN estimates of incidence and mortality worldwide for 36 cancers in 185 countries. CA: a cancer journal for clinicians. 2021 May; 71(3):209-49.

[7]. Ruoslahti E, Bhatia SN, Sailor MJ. Targeting of drugs and nanoparticles to tumors. Journal of cell biology. 2010 Mar 22; 188(6):759-68.

[8]. Bennie LA, McCarthy HO, Coulter JA. Enhanced nanoparticle delivery exploiting tumour-responsive formulations. Cancer nanotechnology. 2018 Dec; 9:1-20.

[9]. Danafar H, Sharafi A, Askarlou S, Manjili HK. Preparation and characterization of PEGylated iron oxide-gold nanoparticles for delivery of sulforaphane and curcumin. Drug research. 2017 Dec; 67(12):698-704.

[10]. Loo SL, Fane AG, Lim TT, Krantz WB, Liang YN, Liu X, Hu X. Superabsorbent cryogels decorated with silver nanoparticles as a novel water technology for point-of-use disinfection. Environmental science & technology. 2013 Aug 20; 47(16):9363-71.

[11]. Salar RK, Sharma P, Kumar N. Enhanced antibacterial activity of streptomycin against some human pathogens using green synthesized silver nanoparticles. Resource-Efficient Technologies. 2015 Dec 1; 1(2):106-15.

[12]. Gade AK, Bonde PP, Ingle AP, Marcato PD, Duran N, Rai MK. Exploitation of Aspergillus niger for synthesis of silver nanoparticles. Journal of Biobased Materials and Bioenergy. 2008 Sep 1; 2(3):243-7.

[13]. Salar RK, Kumar N. Synthesis and characterization of vincristine loaded folic acid–chitosan conjugated nanoparticles. Resource-Efficient Technologies. 2016 Dec 1;2(4):199-214.

[14]. Abbasian M, Roudi MM, Mahmoodzadeh F, Eskandani M, Jaymand M. Chitosan-grafted-poly (methacrylic acid)/graphene oxide nanocomposite as a pH-responsive de novo cancer chemotherapy nanosystem. International journal of biological macromolecules. 2018 Oct 15; 118:1871-9.

[15]. Engineer C, Parikh J, Raval A. Review on hydrolytic degradation behavior of biodegradable polymers from controlled drug delivery system. Trends in Biomaterials & Artificial Organs. 2011 Apr 1; 25(2).

[16]. Kim Y, Park Y, Namkoong S, Lee J. Esculetin inhibits the inflammatory response by inducing heme oxygenase-1 in cocultured macrophages and adipocytes. Food & function. 2014; 5(9):2371-7.

[17]. Chu CY, Tsai YY, Wang CJ, Lin WL, Tseng TH. Induction of apoptosis by esculetin in human leukemia cells. European journal of pharmacology. 2001 Mar 23; 416(1-2):25-32.

[18]. Wang CJ, Hsieh YJ, Chu CY, Lin YL, Tseng TH. Inhibition of cell cycle progression in human leukemia HL-60 cells by esculetin. Cancer letters. 2002 Sep 26; 183(2):163-8.

[19]. Lee SH, Park C, Jin CY, Kim GY, Moon SK, Hyun JW, Lee WH, Choi BT, Kwon TK, Yoo YH, Choi YH. Involvement of extracellular signal-related kinase signaling in esculetin induced G1 arrest of human leukemia U937 cells. Biomedicine & pharmacotherapy. 2008 Dec 1; 62(10):723-9.

[20]. Park C, Jin CY, Kim GY, Choi IW, Kwon TK, Choi BT, Lee SJ, Lee WH, Choi YH. Induction of apoptosis by esculetin in human leukemia U937 cells through activation of JNK and ERK. Toxicology and applied pharmacology. 2008 Mar 1; 227(2):219-28.

[21]. Kuo HC, Lee HJ, Hu CC, Shun HI, Tseng TH. Enhancement of esculetin on Taxol-induced apoptosis in human hepatoma HepG2 cells. Toxicology and applied pharmacology. 2006 Jan 1; 210(1-2):55-62.

[22]. LEE KT, LILLARD DA. Effects of esculetin as a lipoxygenase inhibitor in soybean extracts. Journal of Food Lipids. 1997 Jun; 4(2):119-27.

[23]. Payá M, Halliwell B, and Hoult JR. Interactions of a series of coumarins with reactive oxygen species: scavenging of superoxide, hypochlorous acid and hydroxyl radicals. Biochemical pharmacology. 1992 Jul 22; 44(2):205-14.

[24]. Wang P, Xia YL, Yu Y, Lu JX, Zou LW, Feng L, Ge GB, Yang L. Design, synthesis and biological evaluation of esculetin derivatives as anti-tumour agents. RSC Advances. 2015; 5(66):53477-83.

[25]. Matsunaga K, Yoshimi N, Yamada Y, Shimizu M, Kawabata K, Ozawa Y, Hara A, Mori H. Inhibitory effects of nabumetone, a cyclooxygenase-2 inhibitor, and esculetin, a lipoxygenase inhibitor, on N-methyl-N-nitrosourea-induced mammary carcinogenesis in rats. Japanese journal of cancer research. 1998 May; 89(5):496-501.

[26]. Calvo P, Remunan-Lopez C, Vila-Jato JL, Alonso MJ. Novel hydrophilic chitosan-polyethylene oxide nanoparticles as protein carriers. Journal of applied polymer science. 1997 Jan 3; 63(1):125-32.

[27]. Kakkar P, Das B, Viswanathan PN. A modified spectrophotometric assay of superoxide dismutase.

[28]. Sinha AK. Colorimetric assay of catalase. Analytical biochemistry. 1972 Jun 1; 47(2):389-94.

[29]. Ohkawa H, Ohishi N, Yagi K. Assay for lipid peroxides in animal tissues by thiobarbituric acid reaction. Analytical biochemistry. 1979 Jun 1; 95(2):351-8.

[30]. Prasad M, Salar A, Salar RK. In vitro anticancer activity of curcumin loaded chitosan nanoparticles (CLCNPs) against Vero cells. Pharmacological Research-Modern Chinese Medicine. 2022 Jun 1; 3:100116.

[31]. Shah S, Pal A, Kaushik VK, Devi S. Preparation and characterization of venlafaxine hydrochloride-loaded chitosan nanoparticles and in vitro release of drug. Journal of applied polymer science. 2009 Jun 5; 112(5):2876-87.

[32]. Jain D, Banerjee R. Comparison of ciprofloxacin hydrochloride-loaded protein, lipid, and chitosan nanoparticles for drug delivery. Journal of Biomedical Materials Research Part B: Applied Biomaterials: An Official Journal of the Society for Biomaterials, the Japanese Society for Biomaterials, and the Australian Society for Biomaterials and the Korean Society for Biomaterials. 2008 Jul; 86(1):105-12.

[33]. Neelakandan M, Manoharan S, Muralinaidu R, Thara JM. Tumor preventive and antioxidant efficacy of chlorogenic acid–loaded chitosan nanoparticles in experimental skin carcinogenesis. Naunyn-Schmiedeberg's Archives of Pharmacology. 2023 Mar; 396(3):533-46.

[34]. Shahneh FZ, Valiyari S, Azadmehr A, Hajiaghaee R, Yaripour S, Bandehagh A, Baradaran B. Inhibition of growth and induction of apoptosis in fibrosarcoma cell lines by Echinophora platyloba DC: in vitro analysis. Advances in Pharmacological and Pharmaceutical Sciences. 2013 Jan 1; 2013.

[35]. Koff JL, Ramachandiran S, Bernal-Mizrachi L. A time to kill: targeting apoptosis in cancer. International journal of molecular sciences. 2015 Jan 28; 16(2):2942-55.

[36]. Kurutas EB. The importance of antioxidants which play the role in cellular response against oxidative/nitrosative stress: current state. Nutrition journal. 2015 Dec; 15(1):1-22.

[37]. Li S, Tan HY, Wang N, Zhang ZJ, Lao L, Wong CW, Feng Y. The role of oxidative stress and antioxidants in liver diseases. International journal of molecular sciences. 2015 Nov 2; 16(11):26087-124.

[38]. Kakkar P, Das B, Viswanathan PN. A modified spectrophotometric assay of superoxide dismutase.

[39]. He L, He T, Farrar S, Ji L, Liu T, Ma X. Antioxidants maintain cellular redox homeostasis by elimination of reactive oxygen species. Cellular Physiology and Biochemistry. 2017 Nov 17; 44(2):532-53.

[40]. Gallego MA, Ballot C, Kluza J, Hajji N, Martoriati A, Castera L, Cuevas C, Formstecher P, Joseph B, Kroemer G, Bailly C. Overcoming chemoresistance of non-small cell lung carcinoma through restoration of an AIF-dependent apoptotic pathway. Oncogene. 2008 Mar; 27(14):1981-92.

[41]. Liu K, Liu PC, Liu R, Wu X. Dual AO/EB staining to detect apoptosis in osteosarcoma cells compared with flow cytometry. Medical science monitor basic research. 2015;21:15.

[42]. Adams JM, Cory S. The Bcl-2 apoptotic switch in cancer development and therapy. Oncogene. 2007 Feb;26(9):1324-37.

[43]. Burlacu A. Regulation of apoptosis by Bcl-2 family proteins. Journal of cellular and molecular medicine. 2003 Jul;7(3):249-57.

[44]. Saito M, Korsmeyer SJ, Schlesinger PH. BAX-dependent transport of cytochrome c reconstituted in pure liposomes. Nature cell biology. 2000 Aug;2(8):553-5.

[45]. Vivek R, Thangam R, Nipunbabu V, Ponraj T, Kannan S. Oxaliplatin-chitosan nanoparticles induced intrinsic apoptotic signaling pathway: a “smart” drug delivery system to breast cancer cell therapy. International journal of biological macromolecules. 2014 Apr 1;65:289-97.

[46]. Vivek R, Babu VN, Thangam R, Subramanian KS, Kannan S. pH-responsive drug delivery of chitosan nanoparticles as Tamoxifen carriers for effective anti-tumor activity in breast cancer cells. Colloids and Surfaces B: Biointerfaces. 2013 Nov 1;111:117-23.